Excited State Intramolecular Proton Transfer in Anionic Analogues of Malonaldehyde

Steve Scheiner,* Tapas Kar, and Martin Čuma

Department of Chemistry, Southern Illinois University, Carbondale, Illinois 62901

Received: April 24, 1997; In Final Form: June 16, 1997[⊗]

The transfer of a proton in malonaldehyde takes place within an intramolecular H-bond involving a five-membered ring. This process is compared via ab initio methods with the transfer in analogous systems in which the size of the ring is altered to four and to six and in which the system bears an overall negative charge. In addition to the ground state, calculations are applied to the singlet and triplet $\pi\pi^*$ states, as well as to $^1n\pi^*$ and $^3n\pi^*$. The barriers to proton transfer are found to correlate strongly with various geometric and energetic markers of the strength of the H-bond. The H-bond is weakened by $n \rightarrow \pi^*$ excitation, particularly for the neutral molecule, resulting in a higher transfer barrier. In the case of the two anions, excitation to $^3\pi\pi^*$ strengthens the H-bond, while the result is more ambiguous for the $^1\pi\pi^*$ state. This trend is reversed in malonaldehyde where the singlet is strengthened by the excitation and the triplet weakened. Some of these patterns are traced directly to the nature of the pertinent orbitals and the density shifts arising from the excitation.

Introduction

Proton transfers that take place in the ground electronic states have been investigated over a span of decades, and the process is now rather well understood from both a practical and fundamental perspective.[1] In comparison, excited state proton transfer (ESPT) has received much less attention. A good deal of ESPT work has centered around the transfer of a proton across an intramolecular H-bond in certain situations. Of particular interest have been those molecules in which the absorption occurs at a much higher frequency than the emission that follows the proton transfer, resulting in a large Stokes shift in the fluorescence spectrum.

Systems such as these have found a number of diverse applications including lasers.[2] Additional developing applications that involve ESPT include energy/data storage devices and optical switching,[3] Raman filters and hard-scintillation counters,[4] polymer photostabilizers,[5] and triplet quenchers.[6] On the biological front, it has been suggested that ESPT can aid in understanding the binding properties of protein,[7] or be used as fluorescence probes for biomolecules.[8]

One of the prime features common to many excited-state proton transfers is their rapidity, on the subpicosecond time scale.[9] These fast transfers are commonly attributed to a barrierless process, or at least one with a very low barrier.[10] An important question that arises is therefore how can one account on a fundamental level for the change in the proton transfer barrier that accompanies electronic excitation. And, is a barrier reduction to be expected for all such excitations or are certain excited states more prone to low barriers than others?

There have been a number of ab initio studies that have addressed the ESPT issue.[11,12] The work of Nagaoka's group has been concerned with the difference in energy between the two possible tautomers in molecules like *o*-hydroxybenzaldehyde in its $^1\pi\pi^*$ state.[13] Their ESPT calculations, like many others,[14,15] have largely ignored the energy barriers separating the two minima, and so offer little toward understanding the rapidity of the ESPT. Moreover, these calculations treat only the singlets and so do not address the strong differences occasionally noted between singlets and triplets,[16] nor of states other than $^1\pi\pi^*$. One of the more ambitious attempts to examine an excited state proton transfer to date concerned the [2,2′-bipyridine]-3,3′-diol molecule which contains a pair of OH···N interactions.[14] The large size of the system, containing a pair of aromatic rings, made high-level correlated calculations difficult. While this work was limited to the first triplet, it is useful to note that it reproduced experimental findings of a stability reversal in the two chief tautomers. Moreover, the agreement with experimental vibrational spectra provides optimism that ab initio calculations are indeed useful in studying these systems.

Calculations in this laboratory have been chiefly concerned with molecules like malonaldehyde in which the intramolecular OH···O H-bond completes a five-membered ring of C and O atoms.[17] This work has provided some insights into the properties of the ESPT within a molecule in the absence of complicating solvent effects and free of interactions with a neighboring aromatic system. Replacement of one or more O atoms in malonaldehyde by N has enabled[18] an elucidation of the dependence of the ESPT properties upon the nature of the atoms involved in the H-bond. These calculations have been limited to investigation of H-bonds occurring within five-membered rings. But since the rings containing the intramolecular H-bonds in molecules of practical interest are of varying size, it is important to examine how the number of atoms in the ring influences the ESPT process. For that reason, attention is turned in the present communication to a comparison of the proton transfer in the excited states of the five-membered malonaldehyde molecule, with rings containing both four and six atoms. Another aspect of the system examined here is the total electrical charge on the system. The neutral malonaldehyde molecule is thus compared to systems that contain an overall negative charge, maintaining the malonaldehyde-like conjugation between double bonds within the system.

Methods

The systems examined in this work are illustrated in Figure 1. The five-membered ring of the neutral malonaldehyde molecule is abbreviated by the **5** nomenclature. The smaller and larger rings, each bearing an overall negative charge, are referred to as $\mathbf{4}^-$ and $\mathbf{6}^-$, respectively. The equilibrium

[⊗] Abstract published in *Advance ACS Abstracts,* August 1, 1997.

S1089-5639(97)01387-X CCC: $14.00

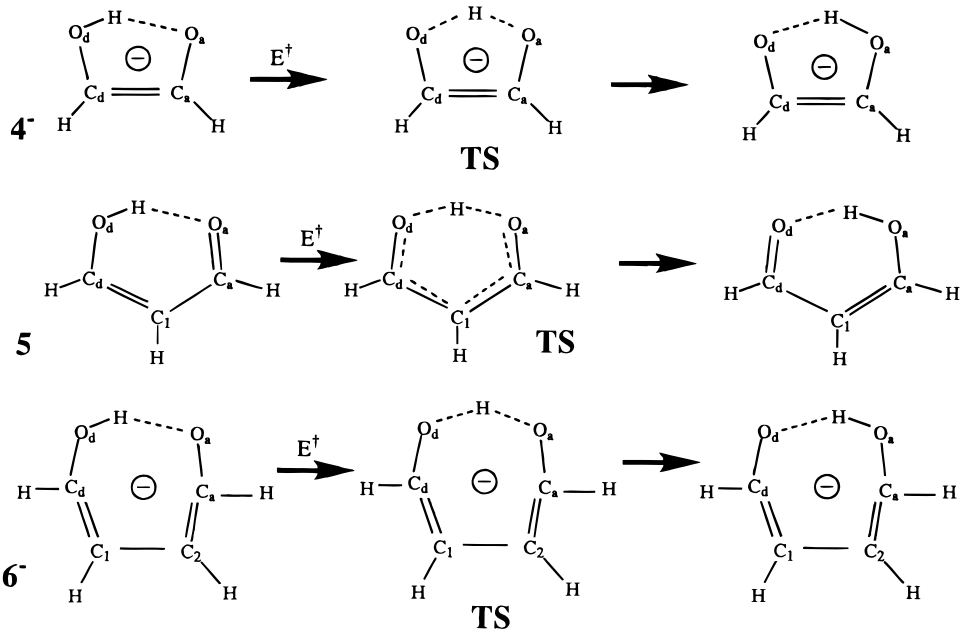

Figure 1. Diagrams showing atomic numbering schemes in the three systems of interest and the formal bonding scheme as the proton transfer progresses. The d subscript refers to the proton donor atom in the equilibrium geometry on the left, and a to the acceptor. TS represents the transition state configuration for proton transfer.

geometries, and the numbering schemes of each, are presented on the left side of Figure 1, along with their formal bonding arrangement, i.e. the placement of single and double bonds. The d and a subscripts are used to indicate the proton donor and acceptor atoms, respectively. The proton transfer passes through a symmetric transition state (TS), over an energy barrier, $E^{\dagger}$. The end point of each transfer is pictured on the right side of Figure 1 and is symmetrically equivalent to the starting point equilibrium geometry. All structures are fully planar throughout.

The GAUSSIAN 94 suite of programs[19] was used to perform the calculations described here. Most calculations made use of the 6-31+G** basis set,[20] although others were implemented as well, as described in detail below. The geometries of the excited states were optimized using the CI singles (CIS) procedure,[21] as implemented in Gaussian. The path of the transfer was monitored by way of the intrinsic reaction coordinate (IRC).[22]

Results

The salient features of the equilibrium geometries of the three species of interest are reported in Table 1. Scanning first the ground states of each, a number of trends become apparent. The C−O bond lengths that refer to the donor group are considerably longer than $r(C_aO_a)$ in all three molecules. This distinction is in keeping with the traditional bonding structure of malonaldehyde, which imparts single- and double-bond character to these two bonds, respectively. But the discrepancy is just as large in the two anions, although both bonds might be considered as having formal single-bond character. The C−O bond lengths are notably longer in the two anions (particularly the four-membered ring) as compared to the neutral malonaldehyde. The C−C bond involving the C_d atom is formally of double type for all three species. This bond becomes progressively shorter as the size of the ring increases. The other C−C bonds are longer, particularly the C_1-C_2 bond in **6**$^-$. It may be noted finally that the patterns of C−C bond lengths in Table 1 conform to the conventional bonding of the three species illustrated in Figure 1. For example, the C_dC_1 and C_2C_a bonds in **6**$^-$ are considerably shorter than C_1C_2, and C_dC_1 in **5** is shorter than C_1C_a.

TABLE 1: Optimized Geometries (Å and deg) of Complexes in Figure 1, Calculated with the 6-31+G Basis Set**[a]

	O_dC_d	C_dC	C_1C_2	CC_a	C_aO_a	$O_d\cdots O_a$	O_dH	$\theta(O_aO_dH)$
				4$^-$				
S_0	1.396	1.350b		1.350b	1.276	2.787	0.948	46.9
$^1\pi\pi^*$	1.315	1.391		1.391	1.232	2.667	0.952	47.9
$^3\pi\pi^*$	1.350	1.521		1.521	1.302	2.568	0.964	35.6
$^1n\pi^*$	1.415	1.417		1.417	1.303	2.844	0.939	51.3
$^3n\pi^*$	1.424	1.441		1.441	1.292	2.873	0.939	51.1
				5				
S_0	1.311	1.345		1.453	1.208	2.689	0.956	27.8
$^1\pi\pi^*$	1.293	1.451		1.423	1.255	2.577	0.983	21.8
$^3\pi\pi^*$	1.351	1.460		1.425	1.223	2.826	0.946	29.7
$^1n\pi^*$	1.341	1.334		1.462	1.258	2.905	0.945	34.3
$^3n\pi^*$	1.346	1.329		1.467	1.255	2.948	0.943	35.2
				6$^-$				
S_0	1.348	1.336	1.486	1.371	1.264	2.647	0.974	8.8
$^1\pi\pi^*$	1.307	1.393	1.391	1.439	1.232	2.572	0.976	8.7
$^3\pi\pi^*$	1.335	1.470	1.389	1.417	1.280	2.541	0.988	6.2
$^1n\pi^*$	1.390	1.356	1.417	1.465	1.277	2.895	0.942	14.4
$^3n\pi^*$	1.393	1.357	1.414	1.480	1.267	2.927	0.941	14.5

[a] Atomic labeling scheme from Figure 1. [b] C_dC and CC_a represent the same (C_dC_a) bond in **4**$^-$.

The last three parameters on the right side of Table 1 deal explicitly with the intramolecular H-bond. As the ring enlarges, there is a clear trend toward a stronger H-bond. That is, $R(O\cdots O)$ becomes progressively shorter, and $r(O_dH)$ elongates, both signs of H-bond strengthening. Another important factor is the easing of strain in the H-bond as the ring enlarges. The nonlinearity of the H-bond, listed in the last column of Table 1, drops from 47° for **4**$^-$, down to only 9° when the ring has expanded to six atoms.

Comparison of the S_o rows in Table 1 with the succeeding rows provides information about the geometry adjustments made as a consequence of electronic excitation. In general, the geometries of the $n\pi^*$ singlet and triplet are quite similar to one another. This behavior contrasts with $\pi\pi^*$ where there are some substantial geometric discrepancies between the singlet and triplet, detailed below.

In all three species, $n \rightarrow \pi^*$ excitation, whether to singlet or triplet, elongates the CO bonds. The C_dO_d stretches increase with the size of the ring, with $\Delta r(C_dO_d)$ exceeding 0.04 Å for

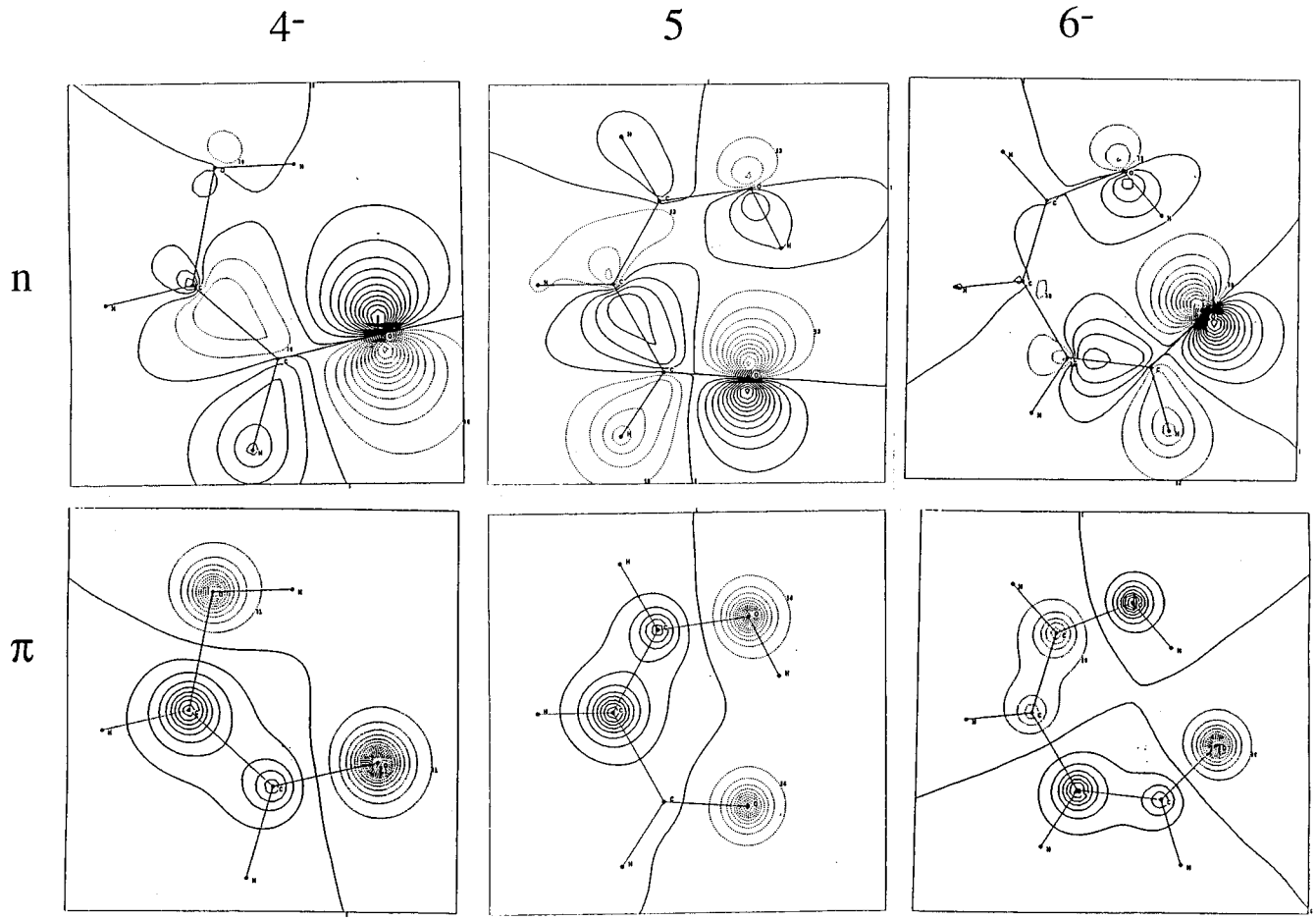

Figure 2. Contour plots of highest occupied n and π orbitals in equilibrium geometries. The amplitude is plotted in the molecular plane for the n MO and 0.1 Å above the plane for the π MO. Regions of positive and negative amplitude are denoted by solid and broken contour lines, respectively. The molecules are oriented so that the proton donor group is at the top and the acceptor near the bottom.

6$^-$. A large elongation is also noted in the C_aO_a bond of **5**. The CC_a bond undergoes a stretch for all three species, especially the two anions. In contrast, the C_dC bond of **5** contracts a bit, whereas this same bond elongates in the two anions.

The character of the orbitals offers some insights into the nature of the geometry changes that accompany the various excitations. The highest occupied n and π MOs that are of most relevance are presented as contour plots in Figure 2. It should be stressed at the outset that these excited states do not represent "pure" excitations from one occupied MO to a single vacant MO. Each state is rather a linear combination of excitations, each from an occupied MO to a vacant one, of pertinent symmetry. For most states, the collection is derived largely from a single occupied MO, but several different vacant orbitals typically make significant contributions. The discussion below attempts to understand the geometry changes on the basis of those particular configurations that are dominant.

Take for example, the C_dO_d stretch that occurs as a result of n $\rightarrow \pi^*$ excitation. As may be seen in Figure 2, the nonbonding orbital from which the electron is excited contains little interaction between these two atoms while the primary π^* orbital has clear antibonding character, consistent with a lengthening of the bond. Similarly for the lengthening of the other CO bond, the n orbital contains some mild antibonding between C_a and O_a, but the antibond in the π^* MO appears to be even stronger.

The character of the n HOMO explains much about the C−C bonding patterns upon n $\rightarrow \pi^*$ excitation. The CC_a bond, for example, undergoes an elongation upon n $\rightarrow \pi^*$ excitation in all three species, especially the two anions. In all three species, the n orbital is largely σ bonding between C_a and its neighboring carbon. It is hence not surprising to see stretches in the CC_a bond for all three when an electron is removed from this MO. The bond between C_d and its neighboring carbon shows opposite trends in **5** and **6**$^-$, shortening in the former and lengthening in the latter, albeit by relatively small amounts. The contraction of the C_1C_2 bond in **6**$^-$ may be connected with π-bonding character of the π^* LUMO to which the electron is excited.

The patterns in the $\pi\pi^*$ states are more erratic, particularly as the singlet and triplet behave quite differently in some cases. For example, the C_aO_a bond is shortened in the $^1\pi\pi^*$ states of **4**$^-$ and **6**$^-$, whereas this bond is lengthened in $^3\pi\pi^*$. Both states yield a contraction in the C_dO_d bond, which may be attributed to the antibonding nature of the interaction between these two atoms in the π HOMO from which the electron is being removed. It is interesting that the magnitude of this shortening is larger in the singlet. The CO bonds of **5** behave differently in that both the singlet and triplet elongate C_aO_a while the C_dO_d bond behaves oppositely for $^1\pi\pi^*$ and $^3\pi\pi^*$. The nodal patterns in the π HOMO may help explain some of this discrepancy. The two anions share a feature that is absent in the neutral molecule: there is an antibond between the C_a and O_a atoms. All three systems show a lengthening of the C_dC bond upon $\pi \rightarrow \pi^*$ excitation, particularly for the triplet. This elongation can be attributed to the partial loss of the bond between these two atoms in the HOMO of all three systems. The CC_a bond, on the other hand, is shortened in **5** but elongated in **6**$^-$ (and **4**$^-$). The π HOMO offers an explanation for this distinction in that there is a bond between C_a and C_2 in **6**$^-$ that is absent in **5**.

TABLE 2: Hydrogen-Bond Energies[a] (kcal/mol) Calculated at the CIS/6-31+G Level**

	4^-	**5**	6^-
S_o	11.1	14.1	24.3
$^1\pi\pi^*$	9.1	23.6	19.1
$^3\pi\pi^*$	11.7	6.7	28.7
$^1n\pi^*$	1.2	2.3	8.4
$^3n\pi^*$	0.9	0.5	6.9

[a] Defined as difference in energy between equilibrium geometry and rotamer with bridging H rotated 180°.

TABLE 3: Excitation Energies (kcal/mol) Calculated with the 6-31+G Basis Set**

	vertical			adiabatic					
	CIS			CIS			MP2		
	4^-	**5**	6^-	4^-	**5**	6^-	4^-	**5**	6^-
$^1\pi\pi^*$	110.5	144.6	108.1	103.8	126.1	90.9	105.8	130.6	109.8
$^3\pi\pi^*$	85.1	80.4	63.7	74.0	56.3	35.8	105.9	109.4	96.9
$^1n\pi^*$	170.4	121.1	159.5	166.9	110.3	141.9	151.9	126.9	156.2
$^3n\pi^*$	163.3	106.7	150.8	158.3	94.5	130.7	157.1	123.0	157.8

The parameters in the last three columns of Table 1 provide information about how a given excitation affects the H-bond strength. R(O···O) is shortened for the $\pi \rightarrow \pi^*$ excitations of both anions and lengthened for the $n \rightarrow \pi^*$ excitations. Consistent with the strengthening or weakening of the H-bond in these two cases, one notes a respective stretch or contraction of $r(O_dH)$. These patterns are also consistent with the linearity markers in the last column of Table 1. Like the anions, **5** also contains the markers of a H-bond weakening for the two $n\pi^*$ states. In contrast, however, the $^3\pi\pi^*$ state would appear to contain a weakened H-bond, as compared to the strengthened interaction in $^1\pi\pi^*$.

The geometric indications of H-bond strength are largely confirmed by energetic criteria. The H-bond energies listed in Table 2 were defined as the difference in energy between the equilibrium configuration of each of the indicated species and the energy of its conformer obtained by rotating the bridging hydrogen atom 180° around the C−O bond axis. It should be stressed that this definition differs from the usual convention in intermolecular cases where the two participating molecules are simply pulled apart. The bond rotation here does of course break the H-bond, but engenders other interactions, e.g. a possible steric repulsion between lone pairs of the two oxygens, that are a factor in the energy difference. Nonetheless, the indicated energy difference does provide some energetic estimate of the strength of the H-bond.

The energetic data in the first row of Table 2 confirm the strengthened H-bond associated with the ring enlargement in the ground state, presumably due in large measure to the relief of strain energy. The singlet and triplet $n\pi^*$ states exhibit the anticipated weakening of the H-bond relative to the ground state by quite substantial amounts; the effects on the triplet are slightly larger than on the singlet. The two $\pi\pi^*$ states behave in a curious fashion. For both of the anions, the H-bond energy is increased, albeit by a relatively small amount, by excitation to the triplet, whereas the singlet shows a weakened interaction. (This weakening of the singlet is opposed to the conclusion one might draw solely on the basis of geometric data in Table 1.) The pattern is opposite in the neutral **5** where it is the triplet that is weakened and the singlet that is nearly doubled in strength, consistent with the geometric data.

Table 3 reports the energies computed to raise each system from its ground state to the indicated excited states. The first three columns refer to vertical excitations in which the geometry of the excited as well as the ground state is frozen in the optimized geometry of the ground state. The adiabatic excitation energies in the next three columns permit the excited state to adopt its most stable geometry following the excitation. Due to the relaxation in the latter case, the adiabatic excitation energies are all smaller than the vertical quantities. The amount of this relaxation energy is variable but is generally greater for the larger species. For example, the 4^- anion has relaxation energies in the range of 3−11 kcal/mol, in contrast to the larger 6^- anion where changes as large as 18−28 kcal/mol appear.

TABLE 4: Proton Transfer Barriers (kcal/mol) Calculated with the 6-31+G Basis Set**

	CIS			MP2		
	4^-	**5**	6^-	4^-	**5**	6^-
S_0	18.1	10.3	5.1	6.8	2.3	1.0
$^1\pi\pi^*$	17.5	4.3	4.1	8.9	−5.8	0.9
$^3\pi\pi^*$	7.2	21.1	2.9	3.6	−0.6	−1.8
$^1n\pi^*$	36.4	23.7	22.6	−2.3	−2.8	−10.7
$^3n\pi^*$	40.9	28.4	27.0	−5.8	0.9	−9.3

As in the case of geometries, the $n\pi^*$ and $\pi\pi^*$ states exhibit qualitatively different behavior. With respect to the $n\pi^*$ states, the neutral **5** has the smallest excitation energies, followed by 6^-. The pattern in the two $\pi\pi^*$ states is different, in that 6^- has the smallest excitation energies, and by quite a wide margin. The $^1\pi\pi^*$ excitation energy of **5** is particularly large, even greater than the two $n\pi^*$ states. In another manner of speaking, the state ordering for the two anions is

$$^3\pi\pi^* < {}^1\pi\pi^* < {}^3n\pi^* < {}^1n\pi^* \quad (1)$$

but the $^1\pi\pi^*$ state breaks this pattern in the neutral **5**, becoming the highest-lying state, higher in energy than both of the $n\pi^*$ states.

Not unexpectedly, correlation makes some sizable contributions to the excitation energies. The last three columns of Table 3 refer to the difference in energy between the ground and excited states at the MP2 level, with geometries of both optimized at the SCF and CIS levels, respectively. Since both the ground and excited states are lowered in energy by correlation, there is no fundamental reason why the addition of correlation will necessarily raise or lower the excitation energy. In fact, both increases and decreases are observed in the data. Most of these quantities are increased by correlation, with the exceptions of two of the four states of 4^- that are reduced. In any case, the addition of correlation does not produce any substantial changes in the energy ordering predicted by the CIS computations. The primary effect of correlation is to reduce the energy difference between the singlet and triplet of a given symmetry. Indeed, the pair of $^3n\pi^*$ and $^1n\pi^*$ states are close together at the MP2 level.

Proton Transfer Barriers. Among issues of primary concern in this work are the barriers to proton transfer in the ground and various excited states. These barriers are reported in Table 4 at both the CIS and MP2 levels. The values for the ground state are consistent with patterns noted previously for intermolecular H-bonds: Adding correlation lowers each barrier by a significant amount,[23] and the barriers drop as the size of the ring increases, due to the accompanying greater strength of the less strained intramolecular H-bond.

The barriers in the excited states exhibit some interesting behavior. Focusing first on the CIS results, one notes quite high barriers for the singlet and triplet $n\pi^*$ states, with the singlet barrier slightly the lower of the two. These high barriers are consistent with the weak H-bonds indicated by the energetics in Table 2 and the geometries in Table 1. As in the case of the ground state, the barriers diminish as the ring enlarges. The $\pi\pi^*$ barriers appear more anomalous at first sight. In the case

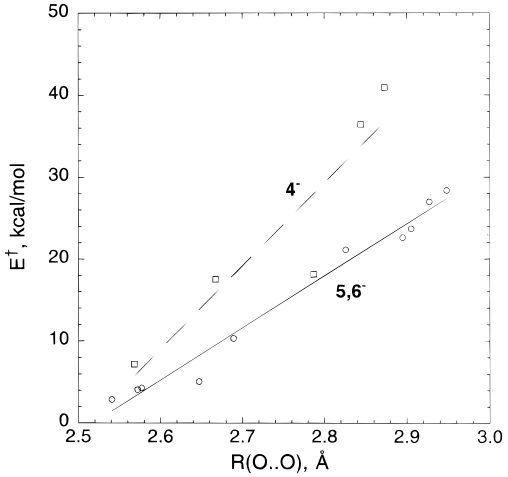

Figure 3. CIS proton transfer barriers as a function of interoxygen separation. The values for the sterically strained **4**$^-$ anion are represented by squares, **5** and **6**$^-$ by the circles. The two sets of data are fit separately by the indicated straight lines.

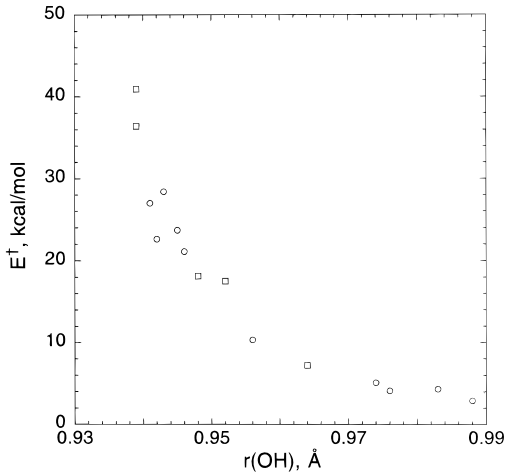

Figure 4. CIS proton transfer barriers as a function of equilibrium value of *r*(OH). The values for the sterically strained **4**$^-$ anion are represented by the squares, **5** and **6**$^-$ by the circles.

of the triplet, the barrier in **5** is quite a bit higher than those of the two anions. This distinction is consistent with the much weaker H-bond in that state for **5** versus **4**$^-$ and **6**$^-$. In the $^1\pi\pi^*$ state, on the other hand, the barrier in **5** is quite low, nearly equal to that in **6**$^-$, again consistent with H-bond patterns, particularly the geometric ones in Table 1.

The close relationship between H-bond character and proton transfer barrier is illustrated in Figures 3 and 4, which compare the barrier with two geometric descriptors of the H-bond. The barriers in the **5** and **6**$^-$ systems, which are less sterically strained than **4**$^-$, obey a very nearly linear relationship between the barrier and the interoxygen distance; the correlation coefficient of the fit is 0.99. Due to its high steric strain, with nonlinearity parameters between 36° and 51°, the barriers in **4**$^-$ are higher than would otherwise be expected on the basis of *R*(O···O). This pattern matches results obtained earlier for a set of protonated diamines, $NH_2(CH)_nNH_3^+$, in which the two amine groups form an intramolecular H-bond.[24] In this case too, wherein the proton is transferring between N atoms, in the ground electronic state, the transfer barrier climbs rapidly as angular strain is imposed on the intramolecular H-bond.

Figure 4 illustrates the interrelationship between the proton transfer barrier and the *r*(OH) bond length. As expected, the stretches in this bond, associated with a stronger H-bond, mark a lower transfer barrier. Note that the steric strain in **4**$^-$ does not prevent these barriers, indicated by the square data points in Figure 4, from nicely coinciding with data for the less strained **5** and **6**$^-$. The data indicate a sharp drop-off in the barrier as *r*(OH) begins to stretch, but this sensitivity declines as the barrier diminishes toward zero. Another geometric factor is the nonlinearity parameter in the last column of Table 1. These angles tend to be larger for the weaker H-bonds of the $^1n\pi^*$ and $^3n\pi^*$ states, with their higher transfer barriers.

TABLE 5: Changes in Geometries (Å and deg) of Complexes in Figure 1 Resulting from Formation of Transition States to Proton Transfer

	O_dC_d	C_dC	C_1C_2	CC_a	C_aO_a	$O_d\cdots O_a$	O_dH	$\theta(O_aO_dH)$
				4$^-$				
S_0	−0.056	−0.007		−0.007	0.064	−0.480	0.273	−27.8
$^1\pi\pi^*$	−0.041	0.046		0.046	0.042	−0.389	0.265	−27.3
$^3\pi\pi^*$	−0.022	0.033		0.033	0.026	−0.272	0.242	−17.7
$^1n\pi^*$	−0.024	−0.050		−0.050	0.088	−0.670	0.235	−29.1
$^3n\pi^*$	−0.035	−0.067		−0.067	0.097	−0.698	0.234	−29.0
				5				
S_0	−0.054	0.050		−0.058	0.049	−0.366	0.233	−15.5
$^1\pi\pi^*$	−0.020	−0.014		0.014	0.018	−0.210	0.224	−10.4
$^3\pi\pi^*$	−0.067	−0.043		−0.008	0.061	−0.475	0.252	−18.6
$^1n\pi^*$	−0.048	0.056		−0.072	0.035	−0.636	0.226	−19.9
$^3n\pi^*$	−0.058	0.063		−0.075	0.033	−0.675	0.230	−20.9
				6$^-$				
S_0	−0.042	−0.012	−0.010	−0.023	0.042	−0.265	0.219	−5.1
$^1\pi\pi^*$	−0.036	0.022	0.001	−0.024	0.039	−0.220	0.203	−4.8
$^3\pi\pi^*$	−0.027	−0.029	−0.008	0.024	0.028	−0.179	0.195	−3.0
$^1n\pi^*$	−0.056	0.035	−0.001	−0.074	0.057	−0.582	0.219	−9.3
$^3n\pi^*$	−0.065	0.039	0.002	−0.084	0.061	−0.609	0.222	−9.5

Another source of information about the proton transfer barrier is derived from the geometry changes that result from the half-transfer of the proton. The data in Table 5 represent the difference in each geometric parameter between the equilibrium structure listed in Table 1 and the structure of the transition state along the proton transfer coordinate. For example, the $O_d\cdots O_a$ column of Table 5 indicates that the motion of the proton toward the middle of the H-bond causes the interoxygen distance to drop. This sort of H-bond shortening that accompanies half proton transfer has been noted on numerous occasions in the past, for both intramolecular and intermolecular H-bonds in their ground state[25] as well as excited states.[12,26] In fact, it is commonly observed that the greatest amount of H-bond contraction is associated with weaker H-bonds, with the highest transfer barriers. This pattern is borne out by the ground and excited state data reported here as well. Note as an example the large *R*(O···O) contractions for the various nπ^* states that are in the range of 0.6−0.7 Å, and it is these states that have the highest transfer barriers. The nearly linear relationship between the equilibrium H-bond length and its degree of contraction upon half proton transfer is exhibited in Figure 5. As in the case of the above relations, the higher strain in the **4**$^-$ system leads to slightly different behavior. In this case, the strain induces a greater degree of H-bond contraction. The correlation coefficient computed for this relationship between *R* and ΔR is 0.97 for **4**$^-$ and 0.99 for the other two systems, characterized by the solid line in Figure 5. The slopes of the fitting lines suggest that each increment by 0.10 Å in the equilibrium H-bond length is associated with an increase in the transfer-induced contraction of 0.12 Å and of 0.14 Å in **4**$^-$. The negative values in the last column of Table 5 illustrate the diminished nonlinearity of the H-bonds as a result of half-transfer of the proton.

The first five columns of data in Table 5 contain information about the changes in bond length within the ring caused by the half-transfer of the proton. In all cases, the departure of the proton causes the O_dC bond to shorten, congruent with a change

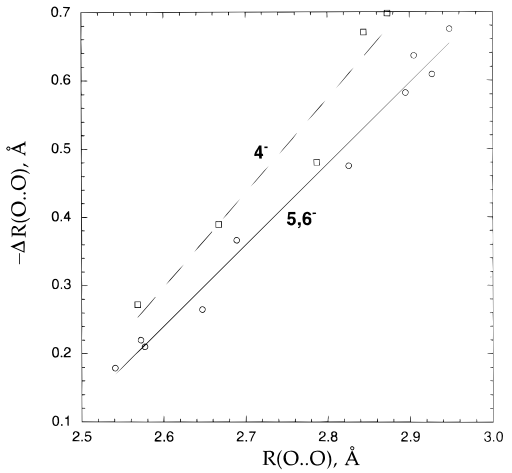

Figure 5. Relationship between the computed equilibrium H-bond length R(O···O) in the various electronic states of the three systems and the amount that this distance contracts as a result of motion of the bridging hydrogen to the O···O midpoint. The values for the sterically strained $\mathbf{4}^-$ anion are represented by the squares, **5** and $\mathbf{6}^-$ by the circles.

in character from single toward double bond. This change is accompanied by a stretch of comparable magnitude in the CO bond of the acceptor group as the approach of the proton tends this bond toward single character.

The C−C bonds of the two anions in their ground state are not very sensitive to proton motion, in contrast to the larger changes in the two C−C bonds in **5**. This distinction may be associated with the observation that the two anions largely retain their basic bonding pattern during proton migration whereas there is a formal reversal of single and double C−C bonds in **5** (see Figure 1).

With respect to the excited states, the nπ* states exhibit the largest alterations in C−C bond lengths. Both singlet and triplet exhibit a contraction of the C−C bond involving C_a, just as in the ground state, only more so. Balancing this contraction out on the other side of the ring, the C_dC bonds in **5** and $\mathbf{6}^-$ are elongated. It is worthy of note as well that the bond length changes in the singlet and triplet nπ* states are quite similar to one another. In contrast, the $^1\pi\pi$* and $^3\pi\pi$* states manifest some intriguing differences. For example, the C_dC bond in $\mathbf{6}^-$ is elongated in the $^1\pi\pi$* state but shortened in $^3\pi\pi$*, with similar opposite behavior in its CC_a bond.

It is possible to extract information about the timing of various geometric changes by monitoring the intrinsic reaction coordinate (IRC). This coordinate represents a mass-weighted steepest-descent path along the potential energy surface from the equilibrium geometry, up over the saddle point in the surface (the transfer transition state), and then down again to the other minimum. Elucidation of the details of this coordinate reveals that the first step in the transfer consists of the contraction of the interoxygen distance. In fact, R(O···O) is roughly equivalent to the IRC for the first 75% or so of the transfer. During this time, the bridging proton moves only slightly away from O_d. It is only when R(O···O) has contracted most of the way toward its ultimate length in the transition state that the bridging proton then undergoes the bulk of its motion toward O_a. This "two-step" character of the proton transfer is true not only of the ground state but for the four excited states as well. The two steps are most clearly separated in the two nπ* states where the bridging proton barely moves at all until R(O···O) has contracted almost completely to its length in the transition state. Previous work[27] has noted a similar partitioning of the coordinate in the $(H_3CH\cdots CH_3)^-$ system which contains a very weak H-bond indeed, as well as in much more strongly bound ionic systems.[28] The changes in the bond lengths within the ring are generally somewhat smoother functions of the IRC, although once again, clear evidence of two separate steps is seen in the singlet and triplet nπ* states.

TABLE 6: Changes in Mulliken Charge of O_a Caused by Indicated Excitation from the Ground State[a]

	$\mathbf{4}^-$	**5**	$\mathbf{6}^-$
$^1\pi\pi$*	0.260	-0.040	0.269
$^3\pi\pi$*	0.096	0.090	0.021
^{1}nπ*	0.642	0.368	0.525
^{3}nπ*	0.650	0.424	0.551

[a] Positive sign corresponds to a loss of electron density as a result of excitation; charges in S_0 are −0.886, −0.598, and −0.841 for $\mathbf{4}^-$, **5**, and $\mathbf{6}^-$, respectively.

The last three columns in Table 4 refer to the proton transfer barriers computed at the MP2 level, using geometries optimized by CIS. Consistent with prior findings,[29,30] electron correlation lowers these transfer barriers. This lowering is particularly large in the case of the nπ* states. The negative values reported for some of these barriers indicate that the MP2 energy of the transition state geometry is lower than that of the equilibrium structure, both optimized at the CIS level. This sort of collapse of the barrier at the MP2 level has been noted in other studies of excited states.[12,26]

Discussion

The results have woven a tight connection between the height of the barrier to proton transfer and the strength of the intramolecular hydrogen bond. It would therefore be instructive to examine those factors involved in electronic excitations that affect the H-bonding interaction.

A dominating feature of the nonbonding MOs in Figure 2 is the high electron density on the proton-acceptor oxygen atom O_a. This density is situated in a region where it is able to accommodate the bridging hydrogen, helping to form the H-bond. It is therefore not surprising that excitation of an electron out of this MO will weaken the H-bond. This supposition is confirmed by the energetic data in Table 2, as well as the geometries in Table 1.

Another marker of this density shift can be gleaned by monitoring the charge assigned to the O_a atom. The changes in Mulliken charge of this atom that are associated with excitation to each of the pertinent excited states are provided in Table 6. (Whereas assignment of total charge to an atom is always arbitrary to a certain extent, it is stressed that what is being presented here is the *change* in charge, typically much less sensitive to basis set or specific method of charge partitioning.) The large positive values listed in the last two rows of Table 6 confirm that indeed the n → π* excitation yields a very sizable shift of electron density away from the proton acceptor atom in all three systems, for both the singlet and triplet. The somewhat smaller values for **5** are likely due to the neutral nature of this molecule, making it less polarizable than the $\mathbf{4}^-$ and $\mathbf{6}^-$ anions.

The O_a charge increments in the two $\pi\pi$* states are revealing as well. A significant loss of density occurs for the singlet states of the two anions, in contrast to a small increase in density in the neutral **5**. This pattern is consistent with the H-bond strength data of Table 2 in that the H-bond of the two anions is weakened by excitation to $^1\pi\pi$* whereas the neutral molecule shows evidence of a bond strengthening. On the other hand, the interoxygen distance is shortened by this excitation in the two anions, just as in the neutral, and the transfer barrier is diminished. It would appear that the geometrical parameters

TABLE 7: H-Bond Energies and Proton Transfer Barriers (kcal/mol) Computed for the Ground State of 4^-

	E_{HB}		$E^\dagger$	
	SCF	MP2	SCF	MP2
4−31G	13.20	14.81	31.47	8.43
6-31G*	11.53	14.29	18.45	7.54
6-31+G*	11.17	13.18	19.33	8.38
6-31+G**	11.05	12.72	18.07	7.25
6-311+G**	10.63	11.95	18.63	7.17

are a better indicator of proton transfer barrier than is the H-bond energy. The weaker accord of the latter quantity may be due to the difficulty in rigorously defining an interaction energy for an intramolecular interaction.

The charge changes in the $^3\pi\pi^*$ state are quite different from those in the singlet, consistent with some of the other discrepant behaviors. For one thing, the triplet does not show much distinction between the neutral molecule and the two anions, as the singlet does. This charge is therefore not a good indicator of transfer barrier in this case, since the excitation to the $^3\pi\pi^*$ state dramatically raises the transfer barrier in the neutral, while acting to diminish the barrier in the anions.

Of course, the charge changes listed in Table 6 cannot fully represent the behavior of the system. For one thing, these charges combine σ and π densities into a single parameter. Hence, it is not expected that the data in Table 6 will provide an excellent indicator of proton transfer barriers in all cases. We find that these charge changes do provide useful indicators of some of the H-bonding and proton transfer behavior of the various systems, especially of the nπ^* states.

In any theoretical elucidation of energetic quantities, one is concerned about the particulars of the basis set. Table 7 provides information about the basis set sensitivity of two key quantities of interest here, the H-bond energy and the barrier to proton transfer. The system under examination is the $\mathbf{4}^-$ anion, and in particular its ground state. All quantities are derived from geometry optimizations at the indicated level of theory. The H-bond energies in the first two columns exhibit a surprisingly low sensitivity to the nature of the basis set. Even the 4-31G set does fairly well, albeit slightly inflating this quantity. Adding polarization functions lowers the H-bond energy, but its calculated value is not much affected by the presence of polarization functions on the hydrogen centers or by diffuse (+) functions on C and O. Note that for any basis set, the inclusion of correlation enhances the H-bond energy by 1 or 2 kcal/mol. The proton transfer barriers reported in the next two columns of Table 7 are also rather insensitive to basis set, with the exception of the inflated 4-31G SCF barrier. All the other basis sets predict SCF barriers in the narrow range of 18−19 kcal/mol. Correlation reduces the barrier by some 10 kcal/mol, providing a best estimate of just over 7 kcal/mol. Another set of calculations[26] has confirmed the insensitivity of transfer barrier to basis set in the ground state of neutral **5**.

The question of basis set sensitivity in the excited states is addressed in Table 8, which lists the transfer barriers for **4-**. Inspecting first the CIS results in the top half of the table, the diffuse (+) functions seem to be important for computation of the $\pi\pi^*$ states, particularly the singlet. On the other hand, there is little sensitivity on the part of the nπ^* states to the presence of polarization or diffuse functions. The MP2 barriers in the lower half of the table suggest that 4-31G is best avoided but that otherwise there is not very much difference between the results of the other basis sets.

Examination of the details of the molecular geometries optimized with each of the various basis sets confirms the conclusions reached on energetic grounds in Tables 7 and 8.

TABLE 8: Proton Transfer Barriers (kcal/mol) Computed for Excited States of 4^-

	$^1\pi\pi^*$	$^3\pi\pi^*$	^{1}nπ^*	^{3}nπ^*
		CIS		
4-31G	9.9	5.8	39.8	42.9
6-31G*	9.9	5.5	42.4	46.9
6-31+G*	18.8	8.5	37.0	41.3
6-31+G**	17.5	7.2	36.4	40.9
6-311+G**	17.8	7.4	37.4	42.4
		MP2		
4-31G	12.2	4.5	5.3	3.0
6-31G*	9.9	3.2	−1.1	−3.4
6-31+G*	10.0	4.8	−0.5	−3.9
6-31+G**	8.9	3.6	−2.3	−5.8
6-311+G**	8.5	3.1	−2.0	−5.6

Of particular relevance, the geometric aspects of the intramolecular H-bond in the various electronic states of $\mathbf{4}^-$ are very similar when compared amongst the 6-31+G*, 6-31+G**, and 6-311+G** basis sets. Analogously, a previous study of the ground state of hydrogen maleate[30] (similar to $\mathbf{6}^-$) compared basis sets ranging from 3-21G to 6-31+G and 6-31G**; all yielded qualitatively similar conclusions. One may conclude, then, that the results described above for the 6-31+G** basis set would probably not be altered in any important way by further refinements of the basis.

Other calculations in the literature are only mildly helpful in assessing the accuracy of this work, as they are generally limited to lower levels of theory and to the ground electronic state. A recent study of the glycolate anion[31] did not incorporate electron correlation. Moreover, this system differs from $\mathbf{4}^-$ here in that the two CH groups are replaced by CH_2, removing the double bonds. The adiabatic barrier to proton transfer (including zero-point vibrational corrections) computed at the SCF/6-31++G** level was 7.3 kcal/mol. A SCF/6-31+G** calculation of the adiabatic transfer barrier in hydrogenoxalate anion $(HOOC-COO)^-$, again in its ground state, is 9.3 kcal/mol.[32]

Perhaps more germane is a recent calculation of the malonaldehyde molecule.[26] Using a 6-311G** basis set, barriers were computed for the $\pi\pi^*$ and nπ^* triplets at the CIS level that are nearly identical to those reported in Table 4, further confirmation of the insensitivity to changes in the basis set. As in our own study, inclusion of correlation via MP2 dramatically reduced these barriers down to nearly zero. Coupled cluster, another means of including correlation, was also tested in this work. The barriers obtained were somewhat dependent upon the particular level of coupled cluster theory but were consistently higher than those obtained by MP2. It is likely, then, that the barriers of the excited states reported on the right side of Table 4 represent underestimates of the true values.

There have been other calculations that lead to questions about the ability of MP2 treatment of correlation, following a CIS calculation, to properly handle ESPT processes.[33] It is for this reason that the MP2 barriers of the excited states have not been emphasized in this report. In any case, the CIS treatment, used for optimizing the geometries of our excited state species, would appear to yield reliable results.[34] The most appropriate means of computing electron correlation in excited states such as these requires further scrutiny and is under current investigation in this laboratory.

Conclusions

The three systems analyzed here differ from one another in certain respects. The size of the ring enlarges from $\mathbf{4}^-$ to **5** to $\mathbf{6}^-$, thereby reducing the strain on the intramolecular H-bond. In fact, geometric and energetic measures of the H-bond confirm

a progressive strengthening in this series. The first and third systems represent anions while **5** is electrically neutral overall. This distinction is reflected in a trend toward stronger H-bonds in the anions, although the aforementioned strain is a major factor as well.

The singlet and triplet nπ* states tend to undergo similar geometry changes upon electronic excitation, in contrast to the $^1\pi\pi$* and $^3\pi\pi$* states that exhibit certain very different properties from one another. The H-bond is weakened by n $\rightarrow$ π* excitation, slightly more so for the triplet than the singlet, and particularly so for the neutral **5** molecule. In the case of the two anions, excitation to $^3\pi\pi$* strengthens the H-bond, while the result is more ambiguous for the $^1\pi\pi$* state. This trend is reversed in **5** where the singlet is clearly strengthened by the excitation and the triplet weakened. Some of these differences appear in the excitation energies as well. For all three systems, $^3\pi\pi$* represents the lowest excited state. For the two anions, the $^1\pi\pi$* state lies only a few kcal/mol higher, whereas this gap is much larger in **5**, making $^1\pi\pi$* the highest lying of the four excited states examined. In all three systems, the singlet and triplet nπ* states lie close to one another. However, the spacing between the two $\pi\pi$* states and the pair of nπ* states is much larger in the two anions.

The indicators of H-bond strength provide useful insights into the height of the energy barrier to proton transfer. One can observe a nearly linear correlation between the barrier and the distance separating the donor and acceptor oxygen atoms in the equilibrium geometry of a particular state. (Due to the high degree of strain in the H-bond of $\mathbf{4}^-$, the barriers in this system are slightly higher than would be otherwise indicated from this correlation.) Another indicator is the equilibrium r(OH) bond length; the strain in $\mathbf{4}^-$ does not introduce any notable discrepancies into this correlation. The shift of the proton to the midpoint of the intramolecular H-bond induces a contraction in R(O$\cdots$O) in all the states examined. The amount of this contraction is in direct proportion to the height of the proton transfer barrier. Also common to all three systems are certain trends in the geometry. The proton transfer causes the CO bond of the donor group to shorten while the acceptor CO bond elongates.

The aforementioned trends are in effect for the anions as well as the neutral molecule under study here. One distinction involves the CC bonds. The bond lengths in the two anions are relatively unaffected by proton motion in the ground state, while there are significant changes in those of the neutral **5**. As in the energetics, the singlet and triplet nπ* states exhibit similar bond length patterns, whereas substantial differences emerge between $^1\pi\pi$* and $^3\pi\pi$*. As in the ground state, proton transfers in the excited states can be dissected into two nearly separable steps. First, the two oxygen atoms move in toward one another, via changes in the ring's internal geometry. It is only after this contraction of R(O$\cdots$O) has been largely completed that the bridging proton moves from one O atom to the acceptor.

The shifting electron density provides certain clues into the fundamental properties of the various states. Excitation of an electron from the highest occupied MO of σ (n) type reduces the density in the lone-pair region of the acceptor oxygen atom. The associated weakening of the H-bond is responsible for the high transfer barriers in the nπ* states. The density loss in the acceptor atom is also reflected in the diminished negative atomic charge upon n $\rightarrow$ π* excitation. Like the H-bond and proton-transfer properties, the charge on the acceptor atom too shows distinctions between the singlet and triplet $\pi\pi$* states.

Acknowledgment. This work was supported by a grant from the National Science Foundation (CHE-9123824).

References and Notes

(1) *Proton-Transfer Reactions*; Caldin, E., Gold, V., Eds.; Halsted Press: New York, 1975, pp 448. Stewart, R. *The Proton: Applications to Organic Chemistry*; Academic Press: Orlando, FL, 1985; Vol. 46, p 313. *Proton Transfer in Hydrogen-Bonded Systems*; Bountis, T., Ed.; Plenum Press: New York, 1992; Vol. Series B: Physics, Vol. 291, p 361. Scheiner, S. *Acc. Chem. Res.* **1985**, *18*, 174. Scheiner, S. *Ibid.* **1994**, *27*, 402.

(2) Chou, P.; McMorrow, D.; Aartsma, T. J.; Kasha, M. *J. Phys. Chem.* **1984**, *88*, 4596. Kasha, M. *Acta Phys. Pol.* **1987**, *A71*, 717. Barbara, P. F.; Walsh, P. K.; Brus, L. E. *J. Phys. Chem.* **1989**, *93*, 29. Ferrer, M. L.; Acuña, A. U.; Amat-Guerri, F.; Costela, A.; Figuera, J. M.; Florido, F.; Sastre, R. *Appl. Opt.* **1994**, *33*, 2266.

(3) Ernsting, N. P.; Nikolaus, B. *Appl. Phys. B.* **1986**, *39*, 155. Parthenopoulos, D. A.; Kasha, M. *Chem. Phys. Lett.* **1988**, *146*, 77. Liphardt, M.; Goonesekera, A.; Jones, B. E.; Ducharme, S.; Takacs, J. M.; Zhang, L. *Science* **1994**, *263*, 367. Douhal, A.; Sastre, R. *Chem. Phys. Lett.* **1994**, *219*, 91.

(4) Martinez, M. L.; Cooper, W. C.; Chou, P.-T. *Chem. Phys. Lett.* **1992**, *193*, 151.

(5) Williams, D. L.; Heller, A. J. *Phys. Chem.* **1970**, *74*, 4473. Heller, H. J.; Blattmann, H. R. *Pure Appl. Chem.* **1973**, *36*, 141. Werner, T.; Woessner, G.; Kramer, H. E. A. In *Photodegradation and Photostabilization of Coatings*; Pappas, S. P., Winslow, F. H., Eds.; American Chemical Society: Washington, DC, 1981; Vol. 151; p 1.

(6) Werner, T. J. *Phys. Chem.* **1979**, *83*, 320. Tarkka, R. M.; Zhang, X.; Jenekhe, S. A. *J. Am. Chem. Soc.* **1996**, *118*, 9438.

(7) Das, R.; Mitra, S.; Nath, D.; Mukherjee, S. *J. Phys. Chem.* **1996**, *100*, 14514. Sytnik, A.; Del Valle, J. C. *Ibid.* **1995**, *99*, 13028.

(8) Sytnik, A.; Kasha, M. *Proc. Nat. Acad. Sci. U.S.A.* **1994**, *91*, 8627. Sytnik, A.; Litvinyuk, I. *Ibid.* **1996**, *93*, 12959.

(9) McMorrow, D.; Dzugan, T. P.; Aartsma, T. J. *Chem. Phys. Lett.* **1984**, *103*, 492. Kasha, M. *J. Chem. Soc., Faraday Trans. 2* **1986**, *82*, 2379. Jang, D.-J.; Brucker, G. A.; Kelley, D. F. *J. Phys. Chem.* **1986**, *90*, 6808. Elsaesser, T.; Schmetzer, B.; Lipp, M.; Bäurle, R. J. *Chem. Phys. Lett.* **1988**, *148*, 112. Grabowska, A.; Mordzinski, A.; Tamai, N.; Yoshihara, K. *Ibid.* **1988**, *1532*, 389. Laermer, F.; Elsaesser, T.; Kaiser, W. *Ibid.* **1988**, *148*, 119. Studer, S. L.; Chou, P. T.; McMorrow, D. *Ibid.* **1989**, *161*, 361. Gormin, D.; Heldt, J.; Kasha, M. *J. Phys. Chem.* **1990**, *94*, 1185. Hineman, M. F.; Brucker, G. A.; Kelley, D. F.; Bernstein, E. R. *J. Chem. Phys.* **1992**, *97*, 3341. Tokumura, K.; Yagata, N.; Fujiwara, Y.; Itoh, M. *J. Phys. Chem.* **1993**, *97*, 6656. Mühlpfordt, A.; Bultmann, T.; Ernsting, N. P.; Dick, B. *Chem. Phys.* **1994**, *181*, 447. Cho, D. W.; Kim, Y. H.; Yoon, M.; Jeoung, S. C.; Kim, D. *Chem. Phys. Lett.* **1994**, *226*, 275. Chudoba, C.; Lutgen, S.; Jentzsch, T.; Riedle, E.; Woerner, M.; Elsaesser, T. *Ibid.* **1995**, *240*, 35. Sarkar, N.; Das, K.; Das, S.; Datta, A.; Nath, D.; Bhattacharyya, K. *J. Phys. Chem.* **1995**, *99*, 17711. Chudoba, C.; Riedle, E.; Pfeiffer, M.; Elsaesser, T. *Chem. Phys. Lett.* **1996**, *263*, 622. Mosquera, M.; Penedo, J. C.; Rodríguez, M. C. R.; Rodríguez-Prieto, F. *J. Phys. Chem.* **1996**, *100*, 5398. Zhang, H.; van der Meulen, P.; Glasbeek, M. *Chem. Phys. Lett.* **1996**, *253*, 97. Douhal, A.; Lahmani, F.; Zewail, A. H. *Chem. Phys.* **1996**, *207*, 477. Douhal, A. *Science* **1997**, *276*, 221. Das, K.; English, D. S.; Petrich, J. W. *J. Am. Chem. Soc.* **1997**, *119*, 2763. English, D. S.; Zhang, W.; Kraus, G. A.; Petrich, J. W. *Ibid.* **1997**, *119*, 2980.

(10) McMorrow, D.; Kasha, M. *J. Phys. Chem.* **1984**, *88*, 2235. Mordzinski, A.; Kühnle, W. *J. Phys. Chem.* **1986**, *90*, 1455. Ernsting, N. P.; Mordzinski, A.; Dick, B. *J. Phys. Chem.* **1987**, *91*, 1404. Brucker, G. A.; Kelley, D. F. *Chem. Phys.* **1989**, *136*, 213. Douhal, A.; Lahmani, F.; Zehnacker-Rentien, A.; Amat-Guerri, F. *J. Phys. Chem.* **1994**, *98*, 12198. Lee, S.-I.; Jang, D.-J. *J. Phys. Chem.* **1995**, *99*, 7537.

(11) Rios, M. A.; Rios, M. C. *J. Phys. Chem.* **1995**, *99*, 12456. Sobolewski, A. L.; Domcke, W. In *The Reaction Path in Chemistry*; D. Heidrich, Ed.; Kluwer Academic: Netherlands, 1995; p 257. Gordon, M. S. *J. Phys. Chem.* **1996**, *100*, 3974. Frank, I.; Grimme, S.; Peyerimhoff, S. D. *Ibid.* **1996**, *100*, 16187. Hass, K. C.; Schneider, W. F.; Estévez, C. M.; Bach, R. D. *Chem. Phys. Lett.* **1996**, *263*, 414.

(12) Guallar, V.; Moreno, M.; Lluch, J. M.; Amat-Guerri, F.; Douhal, A. *J. Phys. Chem.* **1996**, *100*, 19789.

(13) Nagaoka, S.; Nagashima, U.; Ohta, N.; Fujita, M.; Takemura, T. *J. Phys. Chem.* **1988**, *92*, 166. Nagaoka, S.; Nagashima, U. *Chem. Phys.* **1989**, *136*, 153.

(14) Mordzinski, A.; Kownacki, K.; Les, A.; Oyler, N. A.; Adamowicz, L.; Langkilde, F. W.; Wilbrandt, R. *J. Phys. Chem.* **1994**, *98*, 5212.

(15) Chou, P.-T.; Wei, C.-Y.; Chang, C.-P.; Chiu, C.-H. *J. Am. Chem. Soc.* **1995**, *117*, 7259.

(16) Spangler, L. H.; Pratt, D. W. *J. Chem. Phys.* **1986**, *84*, 4789. Tomer, J. L.; Spangler, L. H.; Pratt, D. W. *J. Am. Chem. Soc.* **1988**, *110*, 1615. Tomer, J. L.; Holtzclaw, K. W.; Pratt, D. W.; Spangler, L. H. *J. Chem. Phys.* **1988**, *88*, 1528.

(17) Latajka, Z.; Scheiner, S. *J. Phys. Chem.* **1992**, *96*, 9764. Luth, K.; Scheiner, S. *Int. J. Quantum Chem., Quantum Chem. Symp.* **1993**, *QCS27*, 419. Luth, K.; Scheiner, S. *J. Phys. Chem.* **1994**, *98*, 3582.

(18) Rovira, C.; Scheiner, S. *J. Phys. Chem.* **1995**, *99*, 9854. Duan, X.; Scheiner, S. *Chem. Phys. Lett.* **1993**, *204*, 36. Luth, K.; Scheiner, S. *J. Phys. Chem.* **1995**, *99*, 7352.

(19) Frisch, M. J.; Trucks, G. W.; Schlegel, H. B.; Gill, P. M. W.; Johnson, B. G.; Robb, M. A.; Cheeseman, J. R.; Keith, T. A.; Petersson, G. A.; Montgomery, J. A.; Raghavachari, K.; Al-Laham, M. A.; Zakrzewski, V. G.; Ortiz, J. V.; Foresman, J. B.; Cioslowski, J.; Stefanov, B. B.; Nanayakkara, A.; Challacombe, M.; Peng, C. Y.; Ayala, P. Y.; Chen, W.; Wong, M. W.; Andres, J. L.; Replogle, E. S.; Gomperts, R.; Martin, R. L.; Fox, D. J.; Binkley, J. S.; Defrees, D. J.; Stewart, J. J. P.; Head-Gordon, M.; Gonzalez, G.; Pople, J. A. *GAUSSIAN 94*; Gaussian, Inc.: Pittsburgh, PA, 1995.

(20) Clark, T.; Chandrasekhar, J.; Spitznagel, G. W.; Schleyer, P. v. R. *J. Comput. Chem.* **1983**, *4*, 294.

(21) Foresman, J. B.; Head-Gordon, M.; Pople, J. A.; Frisch, M. J. *J. Phys. Chem.* **1992**, *96*, 135.

(22) Fukui, K. *Acc. Chem. Res.* **1981**, *14*, 363. Gonzalez, C.; Schlegel, H. B. *J. Phys. Chem.* **1990**, *94*, 5523.

(23) Chu, C.-H.; Ho, J.-J. *J. Am. Chem. Soc.* **1995**, *117*, 1076. Bouteiller, Y.; Sadi, S.; Latajka, Z.; Ratajczak, H. *Chem. Phys. Lett.* **1992**, *199*, 55. Latajka, Z.; Scheiner, S. *J. Mol. Struct.: THEOCHEM* **1991**, *234*, 373. Luth, K.; Scheiner, S. *J. Chem. Phys.* **1992**, *97*, 7519.

(24) Duan, X.; Scheiner, S. *J. Am. Chem. Soc.* **1992**, *114*, 5849.

(25) Chu, C.-H.; Ho, J.-J. *J. Phys. Chem.* **1995**, *99*, 16590. Jaroszewski, L.; Lesyng, B.; McCammon, J. A. *J. Mol. Struct.: THEOCHEM* **1993**, *283*, 57. Scheiner, S.; Yi, M. *J. Phys. Chem.* **1996**, *100*, 9235. Cybulski, S.; Scheiner, S. *J. Am. Chem. Soc.* **1987**, *109*, 4199. Latajka, Z.; Scheiner, S. *Int. J. Quantum Chem.* **1986**, *29*, 285.

(26) Barone, V.; Adamo, C. *J. Chem. Phys.* **1996**, *105*, 11007.

(27) Isaacson, A. D.; Wang, L.; Scheiner, S. *J. Phys. Chem.* **1993**, *97*, 1765.

(28) Kar, T.; Scheiner, S. *J. Am. Chem. Soc.* **1995**, *117*, 1344.

(29) Alagona, G.; Ghio, C.; Kollman, P. A. *J. Am. Chem. Soc.* **1995**, *117*, 9855. Cherry, M.; Islam, M. S.; Gale, J. D.; Catlow, C. R. A. *J. Phys. Chem.* **1995**, *99*, 14614.

(30) Rios, M. A.; Rodríguez, J. *Can. J. Chem.* **1993**, *71*, 303.

(31) Smedarchina, Z.; Fernandez-Ramos, A.; Rios, M. A. *J. Chem. Phys.* **1997**, *106*, 3956.

(32) Smedarchina, Z.; Siebrand, W.; Zgierski, M. Z. *J. Chem. Phys.* **1995**, *103*, 5326.

(33) Sobolewski, A. L.; Domcke, W. *Chem. Phys. Lett.* **1993**, *211*, 82. Sobolewski, A. L.; Domcke, W. *Chem. Phys.* **1994**, *184*, 115.

(34) Sobolewski, A. L.; Adamowicz, L. *J. Phys. Chem.* **1995**, *99*, 14277.